Talanta 216 (2020) 120930

Contents lists available at ScienceDirect

Talanta

journal homepage: www.elsevier.com/locate/talanta

A facile biosensor for $A\beta_{40}O$ based on fluorescence quenching of prussian blue nanoparticles

Wenlan Chen[a], Ge Gao[b], Yan Jin[b], Chunyan Deng[a,*]

[a] Hunan Provincial Key Laboratory of Micro & Nano Materials Interface Science, College of Chemistry and Chemical Engineering, Central South University, Changsha, 410083, PR China

[b] Department of Geratology, the Third Xiangya Hospital, Central South University, Changsha, 410013, PR China

ARTICLE INFO

Keywords:
Alzheimer's disease
β-Amyloid oligomers
Prussian blue nanoparticles

ABSTRACT

Amyloid β peptide oligomeFrs (AβOs) have been proved to be crucial biomarkers of Alzheimer's disease (AD). To explore an applicable method for the determination of AβOs is significant for the early AD diagnosis. Prussian blue nanoparticles (PBNPs), as one excellent nanomaterials, have the advantages of good stability, favorable biocompatibility, low cost, easy preparation and controllable shape. PBNPs was found to be of the fluorescence quenching ability to fluorophores, and the adsorption of DNA onto PBNPs surface occurred via the binding of phosphate skeleton in DNA to Fe^{2+}/Fe^{3+} in PBNPs. On basis of this, carboxyl fluorescein (FAM) modified $A\beta_{40}O$-targeting aptamer (FAM-$Apt_{A\beta}$) was adsorbed onto PBNPs. And FAM-$Apt_{A\beta}$@PBNPs-based fluorescent aptasensor for the determination of $A\beta_{40}O$ was developed. Upon incubating FAM-$Apt_{A\beta}$@PBNPs with $A\beta_{40}O$, the fluorescence intensity of the FAM-$Apt_{A\beta}$@PBNPs obviously increased comparing to the initial fluorescence intensity of the FAM-$Apt_{A\beta}$@PBNPs. The changes in the fluorescence intensity of the FAM-$Apt_{A\beta}$@PBNPs were linear with the $A\beta_{40}O$ concentrations ranging from 1.00 nM to 100 nM. Moreover, AD patients and healthy persons can be distinguished using this method to determine $A\beta_{40}O$ concentrations in human cerebrospinal fluid samples from AD patients and healthy persons. It demonstrates that this PBNPs-based aptasensor is not only simple and cost-effective, but also sensitive, selective and more applicable. This fluorescent sensing strategy is promising for the development of aptasensor in clinical fields.

1. Introduction

Alzheimer's disease (AD) is a major cause of progressive dementia for the elderly, has always been the focus of research for decades [1–4]. Though there are continuous debates on the pathogenesis of in AD, it was widely identified that amyloid β peptide (Aβ) aggregates are the neuropathology characteristics of AD [5,6]. The excessive Aβ oligomers (AβOs) can cause a series of pathological damage, eventually leading to the occurrence of AD [7]. AβOs have been reported to be the first indicator of AD [8]. In order to realize the early diagnosis and intervention of AD, more and more researches have proved that the determination of AβOs is meaningful and useful [9]. Many efforts have been made to explore an applicable method for AβO determination [10–12]. But it is challengeable to achieve a simple, sensitive and specific, cost-effective method for sensing AβOs, and therefore for its application in AD early diagnosis.

In the last years, various aptamer-based devices have been explored and reported because aptamers as alternatives to antibodies possess advantages such as ease of engineering and synthesis, good thermal and chemical stability, low molecular weight, low immunogenicity, and etc [13–16]. Among them, fluorescent aptasensors have been attracted more interest because of its inherent ease of operation and high sensitivity [17–20]. Nanomaterials are often used as substrates for sensors [21–25]. These nanomaterials possess excellent fluorescence quenching ability to fluorophores and can strongly adsorb single-stranded DNA (ssDNA) [26–28]. These reported nanomaterial-based fluorescent biosensors have become promising devices with more sensitive and effective application value. However, to further promote the fluorescent biosensor's application in the clinic field requires nanomaterials with advantages of easy synthesis, low cost, good biocompatibility and high stability.

Prussian blue nanoparticles (PBNPs) as an excellent nanomaterial have been widely employed in various fields [29], because of advantages including easy preparation, good stability, biocompatibility, low cost, and controllable shape. It has been synthesized successfully using several methods and for various purposes, including Prussian blue

* Corresponding author.
E-mail address: dengchunyan@csu.edu.cn (C. Deng).

https://doi.org/10.1016/j.talanta.2020.120930
Received 2 February 2020; Received in revised form 9 March 2020; Accepted 12 March 2020
Available online 19 March 2020
0039-9140/ © 2020 Published by Elsevier B.V.

fluorescent part and other applications [30]. PBNPs exhibit great potential as a new generation of photothermal agents alternative to traditional agents, because its superior conversion effect [31]. Moreover, PBNPs as a typical drug in clinic have been approved by USA Food and Drug Administration (FDA) for treatment of radioactive exposure [32]. Thus, PBNPs possess the clinical biosafety for human body. Due to its catalytic activity, PBNPs possess high catalytic activity and have been widely employed to fabricate biosensors and used as nanoenzymes [33]. Additionally, the basic structure of PBNPs is based on the three-dimensional network of iron ions (Fe^{3+}), ferrous ions (Fe^{2+}) and cyanide groups alternately at cubic lattice positions [34]. Valence electrons can be transferred between Fe^{2+} and Fe^{3+} to create an absorption band around 720 nm [35]. For its cubic nanostructure, PBNPs have large specific surface area and high load compared to others. Therefore, it can be deduced that the presence of iron ions (Fe^{3+}) and ferrous ions (Fe^{2+}) may result in DNA strands adsorbing onto PBNPs by the reaction of metal and phosphate skeleton in DNA [36]. Generally, fluorescence resonance energy transfer (FRET) would occur when the fluorescent molecule and the quencher are in close proximity [37]. Metal ions and nanomaterials are often regarded as quenchers in applications, result of energy transduction and the fluorescence intensity changing [38,39]. The conformational variation of FAM-$Apt_{A\beta}$ and PBNPs shorten the distance between the fluorescent molecule (e.g. FAM) and nano-materials (PBNPs), resulting the fluorescence quenching of FAM. Therefore, PBNPs as a potential nanomaterial can be used to fabricate the fluorescent biosensor.

Considering the superiority of PBNPs such as cost-effective and shape-controlled and the significant of AβOs, a rapid and simple fluorescent biosensor for $A\beta_{40}O$ was developed based on the fluorescence quenching effect of PBNPs. FAM-$Apt_{A\beta}$ was served as recognizing elements for $A\beta_{40}O$. FAM-$Apt_{A\beta}$ was absorbed onto PBNPs to form the FAM-$Apt_{A\beta}$@PBNPs. The fluorescence quenching ability of PBNPs to FAM-$Apt_{A\beta}$ was observed. However, upon incubation of $A\beta_{40}O$ with the FAM-$Apt_{A\beta}$@PBNPs solution, the fluorescent signal of FAM-$Apt_{A\beta}$ recovered, which resulted from the binding of FAM-$Apt_{A\beta}$ to $A\beta_{40}O$ and therefore the separation of FAM-$Apt_{A\beta}$ from PBNPs. The determination of $A\beta_{40}O$ was achieved, and furthermore this method is simple, rapid, cost-effective, biocompatible, sensitive and selective. Moreover, the $A\beta_{40}O$ concentrations in cerebrospinal fluid (CSF) samples from AD patients and healthy persons were measured, which is significant for distinguishing AD patients from healthy persons. This work provides a meaningful method for the development of aptasensor in the early diagnosis of AD.

2. Experimental section

2.1. Materials and apparatus

$A\beta_{40}$ and $A\beta_{42}$ were provided by DGpeptides Co., Ltd (Hangzhou, China). The $A\beta_{40}$-targeting carboxyl fluorescein (FAM) modified aptamer (FAM-$Apt_{A\beta}$, 5′-GCCTGTGGTGTTGGGGCGGGTGCGTTTTTTT TTT-3′) was purchased from Shanghai Sangon biotechnology (Shanghai, China). Potassium ferrocyanide ($K_4[Fe(CN)_6]$) and ferric nitrate ($Fe(NO_3)_3$) were obtained from Sigma-Aldrich (St Louis, MO). HEPEs buffer (25.0 mM, pH 7.60) with 100 mM of sodium chloride (NaCl) and 1.00 mM of magnesium chlorides ($MgCl_2$) was used to dissolve $A\beta_{40}O$ and $Apt_{A\beta}$. Millipore ultra-pure water (18.2 MΩ cm) was used to prepare all solutions, which were store at refrigerator at 4 °C.

The fluorescent measurements were conducted on the FL-4600 fluorescence spectrophotometer (Hitachi High-Technology Co., Ltd., Tokyo, Japan). The fluorescence cell quartz used was 350 μL. The experimental parameters are set as following: an excitation wavelength of 470 nm, wavelength range of 490–750 nm, and the slit widths of 10.0 nm. Transmission electron-microscope (TEM) images were conducted on a JEM 2010 (JEOL Company Ltd., Japan). A UV-2450 spectrophotometer (Shimadzu, Kyoto, Japan) was used to monitor UV–visible (UV–vis) spectra. Fourier Transform infrared (FT-IR) spectra were performed by attenuated total reflectance (ATR) in the range of 400–4400 cm^{-1}, with 4.00 cm^{-1} resolution using an Agilent Technologies Cary 630 spectrometer. The Zetasizer Nano ZS Instrument (Marlvern Instruments, Southborough, U.K.) was used for dynamic-light-scattering (DLS) measurements.

2.2. Synthsis of PBNPs and preparation of $A\beta_{40}O$

PBNPs were synthesized by referring to the previous report [40–42]. To begin with, an equal amount of potassium $K_4[Fe(CN)_6]$ and $Fe(NO_3)_3$ were dissolved in water to obtain 1.00 mM $K_4[Fe(CN)_6]$ solution, and 1.00 mM $Fe(NO_3)_3$ solution, respectively. $K_4[Fe(CN)_6]$ solution was heated to 60 °C under stirring. The $Fe(NO_3)_3$ solution was then added dropwise into $K_4[Fe(CN)_6]$ solution over 10.0 min and kept under stirring at 60 °C. The color of the solution changed from colorless to bright blue during mixing. The reaction was kept for 5.00 min and then cooled to room temperature under stirring. The resultant solution was centrifuged at 14,000 rpm for 15.0 min and the precipitate was dispersed into ethanol solution. The procedure of centrifugation/re-dispersion was repeated three times. Finally, the freeze dryer (Virtis Benchtop K, SP Scientific, Gardiner, NY) was used for desiccating it. $A\beta_{40}O$ was prepared according to reports in our previous work [43], and the concentration of $A\beta_{40}O$ solution was calculated as equivalent to the concentration of $A\beta_{40}$ monomer [10].

2.3. Preparation of the FAM-$Apt_{A\beta}$@PBNPs solution

A PBNPs solution (1 mg mL^{-1}) was firstly prepared by dispersing PBNPs power in deionized water, and it was sonicated for 20.0 min before used. To obtain the FAM-$Apt_{A\beta}$@PBNPs solution, various concentrations (50.0, 60.0, 70.0, 80.0, 90.0 μg mL^{-1}) of PBNPs solution were mixed with the FAM-$Apt_{A\beta}$ solution (50.0 nM), and incubating the mixture for 1 h at 25 °C in dark. Subsequently, BSA solutions (500, 700, 900, 1000, 2000 nM) were co-incubated with the FAM-$Apt_{A\beta}$@PBNPs solution to block the free sites on the PBNPs surface.

2.4. Detection of $A\beta_{40}O$

The initial fluorescence intensity (F_0) of FAM-$Apt_{A\beta}$@PBNPs solution was firstly measured. The FAM-$Apt_{A\beta}$@PBNPs solution was used to incubate with $A\beta_{40}O$ solutions with different concentrations for 60.0 min at 25.0 °C in the dark. Afterward, the fluorescence responses (F) of FAM-$Apt_{A\beta}$@PBNPs solution incubated with $A\beta_{40}O$ were measured. The relationship between changes in the fluorescence intensity of FAM-$Apt_{A\beta}$@PBNPs solution ($\Delta F = F–F_0$) induced by $A\beta_{40}O$ and $A\beta_{40}O$ concentrations was investigated.

2.5. Preparation of cerebrospinal fluid samples

CSF samples of AD patients and healthy persons were gotten from the Third Xiangya Hospital of Central South University (Changsha, China). CSF samples were filtered by 30 kDa ultrafiltration membrane to remove the interference of large-scale protein. The resultant samples were stored at −80 °C. Before use, they were diluted with HEPEs (25.0 mM, pH 7.6).

3. Results and discussion

3.1. Principle for $A\beta_{40}O$ detection

The construction and principle of the PBNPs-based aptasensor for $A\beta_{40}O$ is illustrated in Fig. 1. Herein, FAM modified $Apt_{A\beta}$ (FAM-$Apt_{A\beta}$) and PBNPs are involved. Cubic shaped PBNPs are firstly synthesized. The three-dimensional network of iron ions (Fe^{3+}), ferrous ions (Fe^{2+}) and cyanide groups (CN^-) are at cubic lattice positions [34]. FAM-

$Apt_{Aβ}$ is absorbed onto the surface of PBNPs because of the binding of phosphate skeleton of FAM-$Apt_{Aβ}$ to Fe^{2+}/Fe^{3+} in PBNPs [36]. The prepared FAM-$Apt_{Aβ}$@PBNPs serves as the fluorescent probe-FAM-$Apt_{Aβ}$@PBNPs for $Aβ_{40}O$. For the FAM-$Apt_{Aβ}$@PBNPs, there is negligible fluorescence signal observed due to fluorescence quenching ability of PBNPs to FAM. However, after incubating the FAM-$Apt_{Aβ}$@PBNPs solution with $Aβ_{40}O$, the binding of $Aβ_{40}O$ to $Apt_{Aβ}$ occurs, resulting in the separation of the fluorophore from the PBNPs surface. And an obvious enhancement in fluorescence intensity of the FAM-$Apt_{Aβ}$@PBNPs solution produces. Therefore, this strategy is not only fabrication-simple and cost-effective, but also feasible for the detection of $Aβ_{40}O$ with high sensitivity and selectivity. The PBNPs-based fluorescent sensing plays a potential role in exploring the method for the early diagnosis of diseases.

3.2. Characterization of PBNPs and FAM-$Apt_{Aβ}$@PBNPs

DLS and TEM techniques are used to characterize PBNPs. As shown in Fig. 2-A, DLS result demonstrates that the size of PBNPs is ca. 68 nm, which is a hydrodynamic diameter (hydrated state). TEM image of PBNPs displayed in Fig. 2-B illustrates that the synthesized PBNPs are cubic-shaped and uniformly dispersed, the size is ca. 50 nm, which is the actual size at the dried state of sample. These results are consistent with reports [40], and indicate the successful synthesis of PBNPs.

Additionally, PBNPs and the FAM-$Apt_{Aβ}$@PBNPs are further investigated by the FT-IR spectra. As shown in Fig. 2-C, bands at 3430 cm^{-1} and 1639 cm^{-1} are attributed to νOH and δOH of crystal water [44], respectively (curve a). 2084 cm^{-1} band belongs to νCN of PBNPs, 490 cm^{-1} and 600 cm^{-1} bands are due to νFe-C or νFe-C═N [45]. These results further indicate the successful synthesis of PBNPs. Seen in Fig. 2-b, the band at 1040 cm^{-1} could be derived from $ν_{as}PO$ in the phosphate skeleton of FAM-$Apt_{Aβ}$ [46], which confirms that the successful adsorption of $Apt_{Aβ}$ onto PBNPs. Moreover, the appearance of band at 1186 cm^{-1} could be explained by the performance of metal-phosphate bond between FAM-$Apt_{Aβ}$ and PBNPs [47]. This indicates the adsorption of $Apt_{Aβ}$ onto PBNPs due to the binding of phosphate skeleton of FAM-$Apt_{Aβ}$ to Fe^{2+}/Fe^{3+} in PBNPs.

Additionally, in order to prove the stability of the FAM-$Apt_{Aβ}$@PBNPs, UV–vis characterizations of PBNPs and the FAM-$Apt_{Aβ}$@PBNPs are carried out, respectively. From Fig. 2-D, an UV–vis spectra with a maximum absorption at 720 nm is observed, which is the characteristic adsorption peak of PBNPs [48]. Similarly, the maximum absorption the FAM-$Apt_{Aβ}$@PBNPs solution is at 720 nm. This elucidates that the immobilization of FAM-$Apt_{Aβ}$ onto PBNPs cannot affect the basic structure of PBNPs. All these results indicate the formation and stability of the FAM-$Apt_{Aβ}$@PBNPs.

3.3. Feasibility of the fluorescent aptasensor

Fig. 3 displays the fluorescence intensities of FAM-$Apt_{Aβ}$, the FAM-$Apt_{Aβ}$@PBNPs before and after treated with $Aβ_{40}O$ solution. FAM-$Apt_{Aβ}$ has an obvious fluorescence signal (curve a). However, the FAM-$Apt_{Aβ}$@PBNPs shows a negligible fluorescence emission at 520 nm (curve b), which indicates that the successful adsorption of FAM-$Apt_{Aβ}$ onto PBNPs surface. It also indicates the quenching ability of PBNPs to FAM. Upon $Aβ_{40}O$ solutions (30.0 nM, 50.0 nM, 80.0 nM) were incubated with the FAM-$Apt_{Aβ}$@PBNPs solution, the fluorescence intensities of the FAM-$Apt_{Aβ}$@PBNPs obviously enhanced (curves c, d, e). The fluorescence recovery of FAM-$Apt_{Aβ}$ results from the specific binding of $Aβ_{40}O$ to FAM-$Apt_{Aβ}$ and therefore the separation of FAM-$Apt_{Aβ}$ from PBNPs surface. This FAM-$Apt_{Aβ}$@PBNPs based strategy is feasible for the detection of $Aβ_{40}O$.

3.4. Optimization of experiments

3.4.1. Molar ratio between FAM-$Apt_{Aβ}$ and PBNPs

For the FAM-$Apt_{Aβ}$@PBNPs system, the optimal ratio between FAM-$Apt_{Aβ}$ and PBNPs is essential for the sensor's sensitivity and reproducibility. In this work, a 50 nM FAM-$Apt_{Aβ}$ solution was used to incubate with different concentration of PBNPs solution to prepare the FAM-$Apt_{Aβ}$@PBNPs solutions. And the fluorescent intensities of the FAM-$Apt_{Aβ}$@PBNPs solutions were determined, as shown in Fig. 4-A. It was observed that the fluorescent intensities of the resultant solutions decrease with PBNPs concentration increasing from 50.0 to 90.0 μg mL^{-1}, and reaching a plate up to 90.0 μg mL^{-1}. This demonstrates that 90.0 μg mL^{-1} PBNPs can ensure the optimal quenching of 50.0 nM FAM-$Apt_{Aβ}$. Therefore, 50.0 nM FAM-$Apt_{Aβ}$ and 90.0 μg mL^{-1} PBNPs solutions are chosen to prepare the FAM-$Apt_{Aβ}$@PBNPs.

3.4.2. BSA concentration

BSA was chosen to block PBNPs unbounded sites and to avoid competitive adsorption of other-existing substances. A series of concentrations of BSA (500, 700, 900, 1000, 2000 nM) were incubated with the FAM-$Apt_{Aβ}$@PBNPs solution and Fig. 4-B showed the fluorescence intensities of the resultant solutions. It can be seen that when BSA concentration was up to 700 nM, the fluorescence signal of the FAM-$Apt_{Aβ}$@PBNPs tend to recover. This demonstrates that 700 nM BSA was the most suitable for blocking PBNPs unbounded sites.

3.4.3. Temperature, reaction time and pH

The effect of temperature and reaction time were systematically investigated. Fig. 5-A shows the fluorescent responses of the FAM-$Apt_{Aβ}$@PBNPs to 100 nM $Aβ_{40}O$ under different temperatures (4 °C, 15 °C, 25 °C, 37 °C). It is observed that the reaction temperature has a distinct impact on the fluorescence intensities of the FAM-$Apt_{Aβ}$@PBNPs, and 25 °C is suitable for higher detection sensitivity. The reaction time (0 min, 20 min, 40 min, 60 min, 80 min) for the specific binding of the FAM-$Apt_{Aβ}$@PBNPs to $Aβ_{40}O$ was also optimized, as shown in Fig. 5-B. It is found that the fluorescence intensities of the FAM-$Apt_{Aβ}$@PBNPs increase as time going on, and reaching the maximum after 60 min. Thus, 60 min is enough for the incubation of $Aβ_{40}O$ with the FAM-$Apt_{Aβ}$@PBNPs.

Fig. 5-C clearly indicates that the accuracy of detection is obviously affected by pH, and the highest fluorescence intensity is obtained at pH 7.6. This is due to that acidity affect the secondary structure and active site of the protein [49]. Therefore, 25 °C, 60 min and pH 7.6 are selected as the optimal conditions.

3.5. Sensing for $Aβ_{40}O$

Under optimal conditions, the analytical performance of this proposed aptasensor was investigated. Fig. 6-A shows the fluorescent responses of the FAM-$Apt_{Aβ}$@PBNPs to various concentrations of $Aβ_{40}O$. It is observed that the fluorescence intensities of the FAM-$Apt_{Aβ}$@PBNPs gradually enhance with $Aβ_{40}O$ concentrations increasing from 1.00 to 200 nM. Fig. 6-B displays the calibration curve of $Aβ_{40}O$ concentrations ($c_{Aβ40O}$) with ΔF. ΔF is linearly relative to $c_{Aβ40O}$ from 1.00 to 100 nM, and the linear equation is $\Delta F = 5.45\ c_{Aβ40O}/\text{nM} + 8.57$ ($R^2 = 0.996$). This elucidates that the proposed aptasensor for $Aβ_{40}O$ determination is feasible and highly sensitive. Additionally, comparing to the representative sensors for AD biomarkers shown in Table 3, it can be concluded that this present sensor's performance is comparative or better in sensitivity and accuracy.

3.6. Specificity assay and recovery test

To examine the specificity of this proposed aptasensor, $Aβ_{40}M$, $Aβ_{42}M$, $Aβ_{42}O$ were chosen as possible interferents for the determination of $Aβ_{40}O$. Under the optimized experimental conditions, $Aβ_{40}M$

(5.00 μM), $A\beta_{42}M$ (5.00 μM), $A\beta_{42}O$ (5.00 μM) and $A\beta_{40}O$ (50.0 nM) were incubated with the FAM-$Apt_{A\beta}$@PBNPs solution, respectively. As shown in Fig. 7, even if the concentrations of $A\beta_{40}M$, $A\beta_{42}M$, $A\beta_{42}O$ are much higher than that of $A\beta_{40}O$, their ΔF are still negligible. This manifests that the aptasensor possesses high specificity.

In order to assess the accuracy of this proposed aptasensor, the recovery rates of $A\beta_{40}O$ spiked in ACSF were tested. As displayed in Table 1, the recovery rates of $A\beta_{40}O$ (30.0 nM, 40.0 nM, 60.0 nM) spiked in ACSF are 99.6%, 114%, 98.8%, respectively. This proves the high specificity of this developed aptasensor.

3.7. Testing $A\beta_{40}O$ in CSF from AD patients and healthy persons

To further verify the applicability of our proposed aptasensor, the determination of $A\beta_{40}O$ in CSF samples has been performed. As shown in Table 2. $A\beta_{40}O$ concentrations in three AD patients' CSF samples are 15.0 nM, 40.0 nM, and 74.7 nM, respectively. However, $A\beta_{40}O$ concentrations in three healthy persons' CSF samples are 4.39 nM, 6.07 nM and 8.26 nM, respectively, which are lower than those of AD patients. Our proposed sensor not only can determine the concentrations of $A\beta_{40}O$ in real CSF samples, but also may distinguish healthy persons from AD patients. This fluorescent aptasensor is applicable and reliable for the determination of $A\beta_{40}O$ in CSF samples.

4. Conclusions

In this work, a fluorescent aptasensor for the determination of $A\beta_{40}O$ has been developed based on the quenching ability of PBNPs to the absorbed FAM-$Apt_{A\beta}$. Its simple operations and extremely low cost made the detection method advantageous over many tedious and costly diagnostics. Moreover, the method has been demonstrated to be sensitive to detect $A\beta_{40}O$ with the lowest detectable concentration of 1.00 nM $A\beta_{40}O$. $A\beta_{40}O$ can be specifically identified by the proposed strategy among $A\beta_{40}M$, $A\beta_{42}M$, $A\beta_{42}O$. More significantly, the determination of $A\beta_{40}O$ in CSF samples from AD patients and healthy persons has been successfully achieved in this method. According to the obtained results, and AD patients and healthy persons may be distinguished. This sensing strategy lays a potential foundation for developing a simple, cost-effective, sensitive, selective and applicable method for the early diagnosis of AD. This work is essential for the development of the PBNPs-based fluorescent biosensor.

CRediT authorship contribution statement

Wenlan Chen: Investigation, Data curation, Writing - original draft. **Ge Gao:** Conceptualization, Investigation, Writing - original draft, Writing - review & editing. **Yan Jin:** Conceptualization, Investigation, Writing - original draft, Writing - review & editing. **Chunyan Deng:** Conceptualization, Investigation, Writing - original draft, Writing - review & editing.

Declaration of competing interests

The authors declared that they have no conflicts of interest to this work.

Acknowledgements

This work was financially supported by the National Natural Science Foundation of China (21727810, 21573290, 21005090).

Appendix

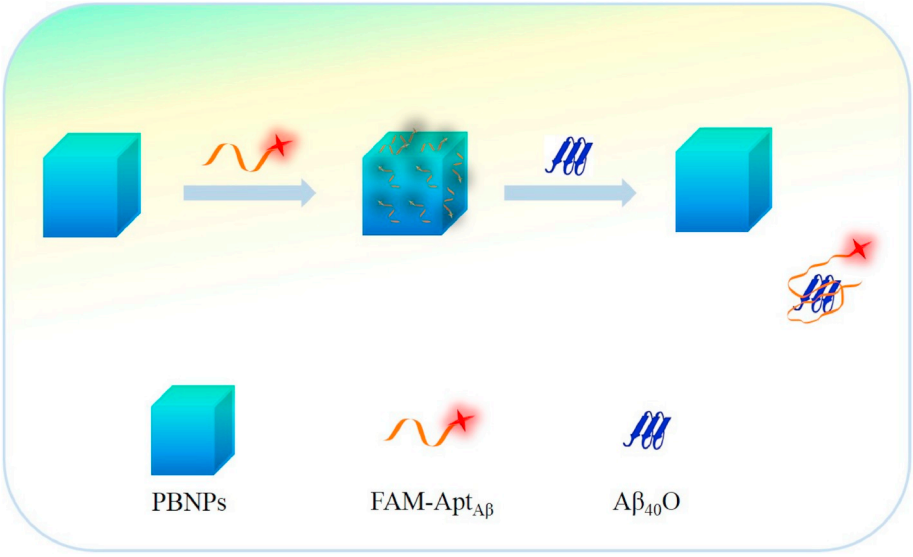

Fig. 1. The construction and principle of the fluorescent aptasensor for $A\beta_{40}O$

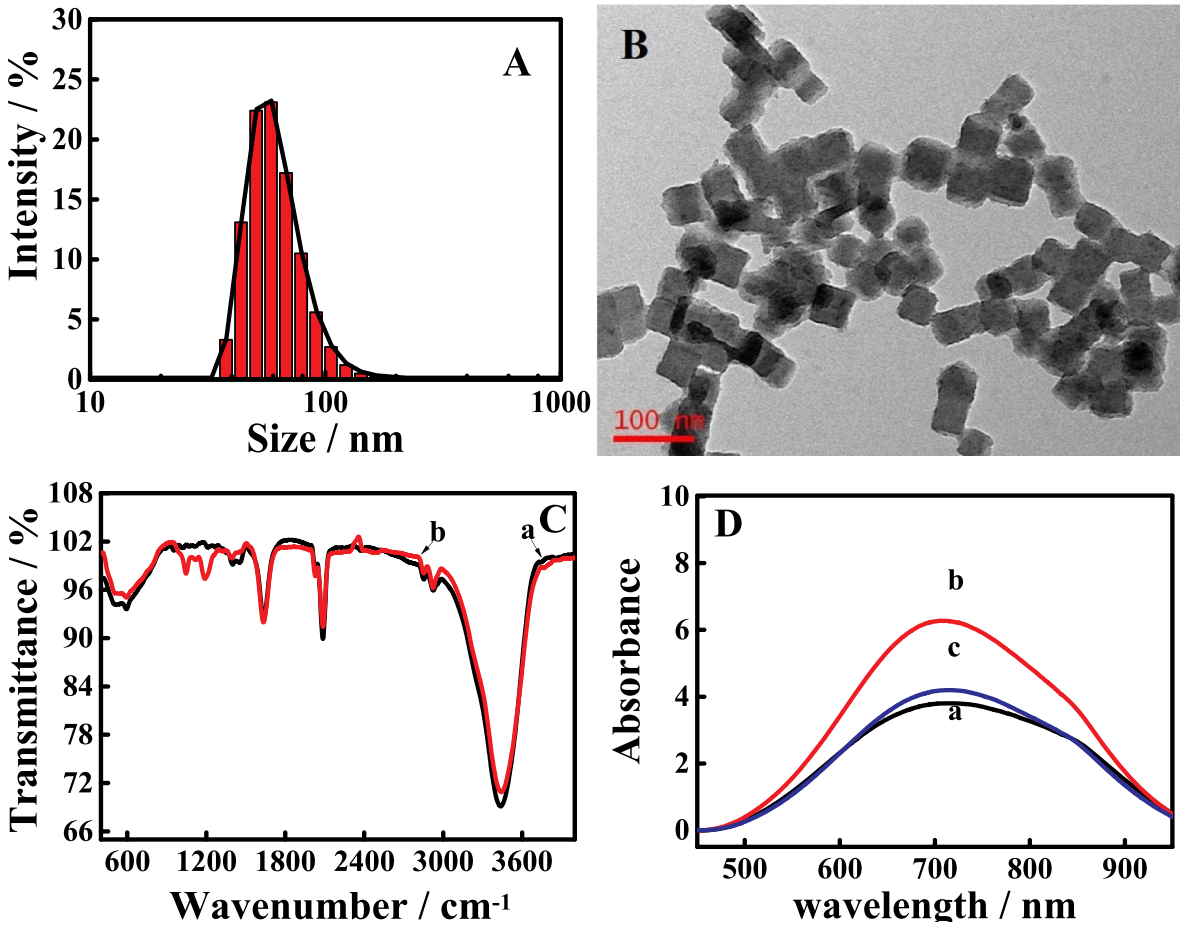

Fig. 2. DLS (A) and TEM images (B) of PBNPs. (C) FT-IR spectra of PBNPs (curve a), and FAM-Apt$_{A\beta}$@PBNPs (curve b). (D) UV–vis spectra of PBNPs (curve a), and FAM-Apt$_{A\beta}$@PBNPs (curve b) and Aβ_{40}O/FAM-Apt$_{A\beta}$@PBNPs (curve c) in HEPEs buffer (25.0 mM, pH 7.6) solution.

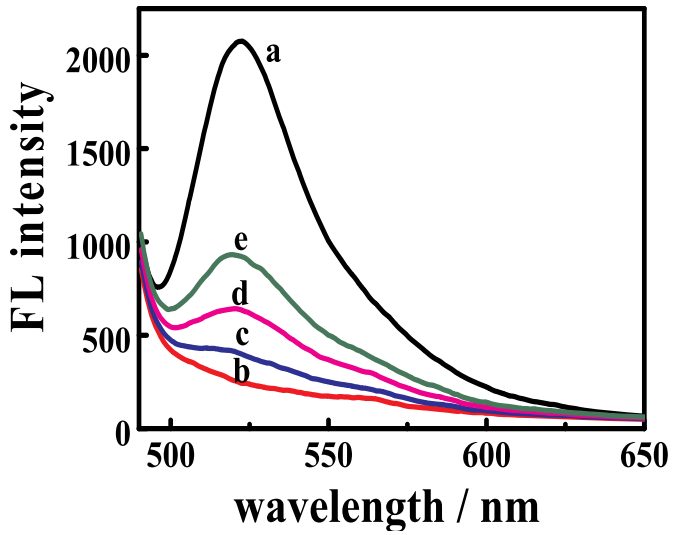

Fig. 3. The fluorescence intensities of FAM-Apt$_{A\beta}$ (a), FAM-Apt$_{A\beta}$@PBNPs before (b) and after incubation with 30.0 nM, 50.0 nM, 80.0 nM Aβ_{40}O (c, d, e).

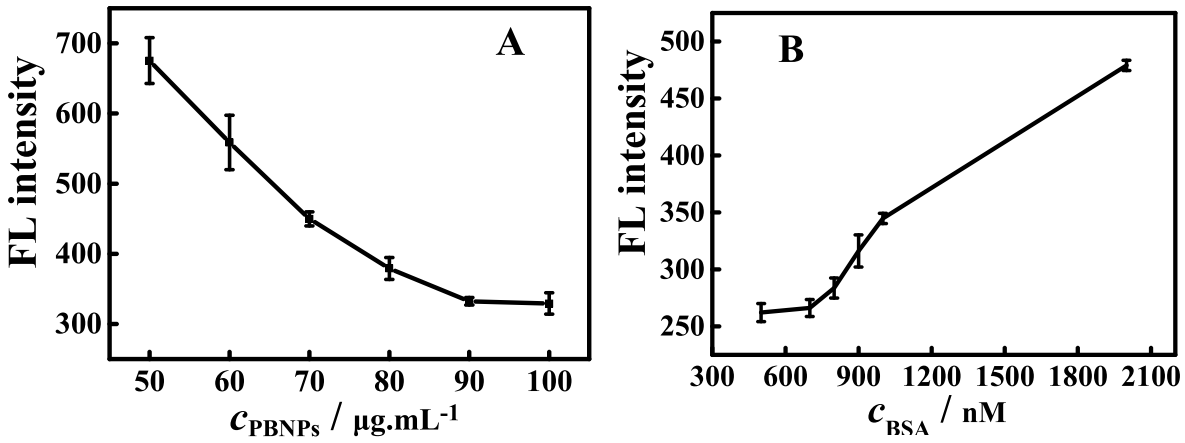

Fig. 4. (A) The fluorescence intensities of FAM-Apt$_{Aβ}$ in the presence of various concentrations PBNPs (50.0, 60.0, 70.0, 80.0, 90.0, 100 μg mL^{-1}), 50.0 nM Apt$_{Aβ}$. (B) The fluorescence intensities of FAM-Apt$_{Aβ}$@PBNNPs caused by incubation with BSA (500, 700, 800, 900, 1000, 2000 nM). Error bars were calculated from three replicate measurements.

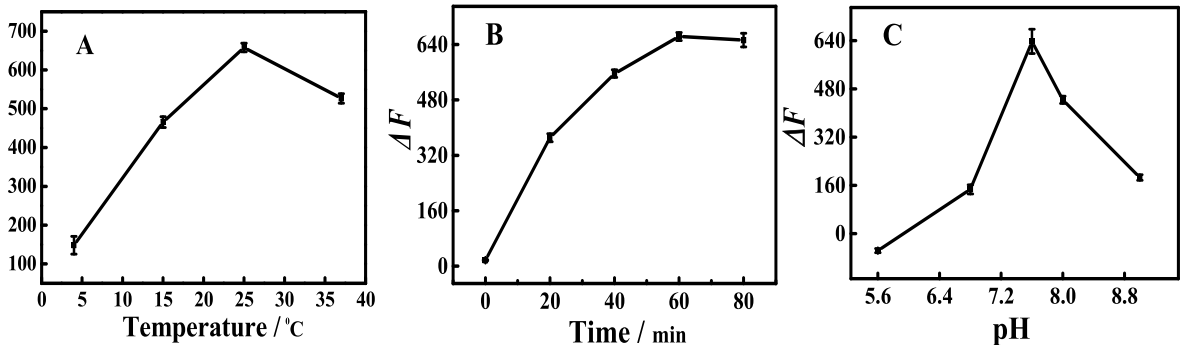

Fig. 5. The effect of temperature (A), reaction time (B) and pH (C) on fluorescent responses of FAM-Apt$_{Aβ}$@PBNNPs to 50.0 nM Aβ$_{40}$O. Error bars were calculated from three replicated measurements.

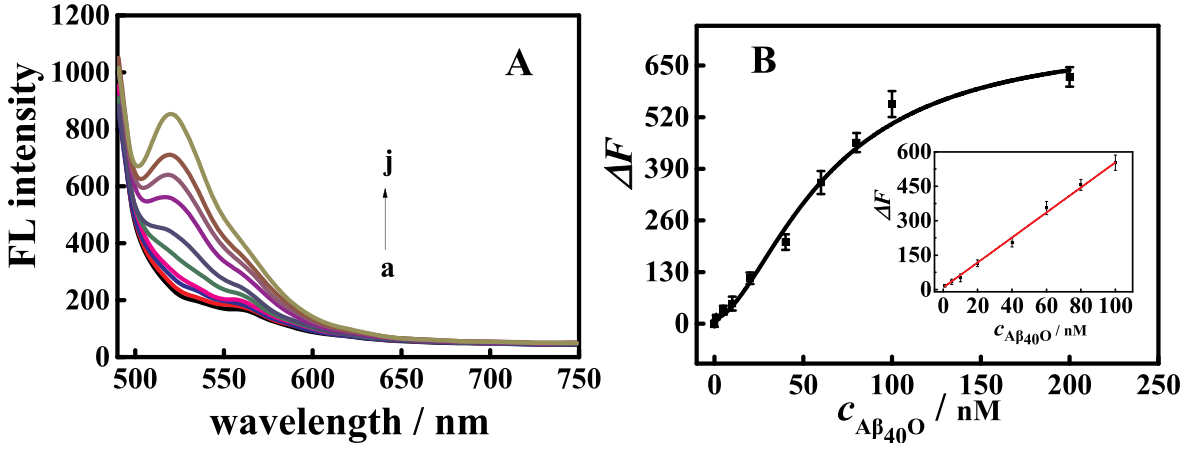

Fig. 6. (A) The fluorescence intensities of FAM-Apt$_{Aβ}$@PBNPs after incubated with various concentrations of Aβ$_{40}$O in 25.0 mM HEPEs (pH 7.60) (B) The corresponding relationships between Δ*F* and Aβ$_{40}$O concentrations. The inset shows the linear relationships between Δ*F* and $c_{Aβ40O}$. Error bars were calculated from three replicated measurements.

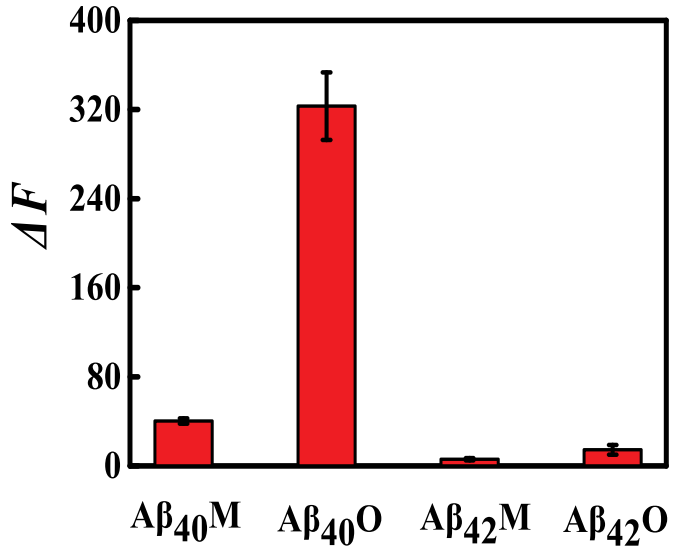

Fig. 7. Selectivity of this proposed aptasensor. Δ*F* of the FAM-Apt$_{Aβ}$@PBNPs to 50 nM A$β_{40}$O, 5.00 μM A$β_{40}$M, 5.00 μM A$β_{42}$M, 5.00 μM A$β_{42}$O, respectively. Error bars were calculated from three replicated measurements.

Table 1
Recoveries of A$β_{40}$O added in ACSF samples.

Sample	Addition(nM)	Recovered(nM)	RSD(%)	Recovery(%)
1	30.0	29.9 ± 2.3	7.7	99.6
2	40.0	45.4 ± 2.3	5.1	114
3	60.0	59.3 ± 2.7	4.6	98.8

Table 2
Detection of A$β_{40}$O in 20-fold diluted CSF samples from AD patients and healthy persons, respectively.

Sample		Detection amount (nM)	RSD(%)
Healthy persons	1	4.39 ± 0.26	2.50
	2	6.07 ± 1.62	3.10
	3	8.26 ± 0.65	2.80
AD Patients	1	15.0 ± 0.41	2.70
	2	40.0 ± 0.47	0.990
	3	74.7 ± 0.47	5.10

Table 3
Comparison of representative sensors examples for AD biomarkers.

Detection strategy	Detection range	Detection limit	Characteristic	Ref.
AuNPs based Colorimetry	35.0–700 nM	10.0 nM	Rapid but less-accurate	[10]
Curcumin-Ni based Electrochemistry	0.001–5 nM	1.00 pM	Sensitive but complicated	[50]
AuNPs based SPR	0.02–1.00 nM	20.0 pM	Regenerable but costly	[51]
N-terminal Aβ antibody based ELISA	1.00–800 pM	1.00 pM	Sensitive but chronical	[52]
PBNPs based Fluorescence	1.00–100 nM	1.00 nM	Simple and cost-effective	this work

Appendix A. Supplementary data

Supplementary data to this article can be found online at https://doi.org/10.1016/j.talanta.2020.120930.

Novelty Statement

Amyloid β peptide oligomers (AβOs) have been proved to be crucial biomarkers of Alzheimer's disease (AD). To explore an applicable method for the determination of AβOs is significant for the early AD diagnosis. Prussian blue nanoparticles (PBNPs), as one excellent nanomaterials, have the advantages of good stability, favorable biocompatibility, low cost, easy preparation and controllable shape. PBNPs was found to be of the fluorescence quenching ability to fluorophores, and the adsorption of DNA onto PBNP surface occurred via the binding of phosphate skeleton in DNA to Fe2+/Fe3+ in PBNPs. On basis of this, Carboxyl fluorescein (FAM) modified Aβ40O-targeting aptamer (FAM-AptAβ) was adsorbed onto PBNPs.

And FAM-AptAβ@PBNPs-based fluorescent aptasensor for the determination of Aβ40O was developed. Upon incubating FAM-AptAβ@PBNPs with Aβ40O, the fluorescence intensity of the FAM-AptAβ@PBNPs obviously increased comparing to the initial fluorescence intensity of the FAM-AptAβ@PBNPs. The changes in the fluorescence intensity of the FAM-AptAβ@PBNPs were linear with the Aβ40O concentration ranging from 1.00 nM to 100 nM. Moreover, AD patients and healthy persons can be distinguished using this method to determine Aβ40O concentrations in human cerebrospinal fluid samples from AD patients and healthy persons. It demonstrates that this PBNPs-based aptasensor is not only simple and cost-effective, but alsosensitive, selective and more applicable. This fluorescent sensing strategy is promising for the development of aptasensor in clinical fields.

References

[1] Y.W. Zhang, R. Thompson, H. Zhang, H. Xu, APP processing in Alzheimer's disease, Mol. Brain Res. 4 (2011) 1–13.

[2] M. Padurariu, A. Ciobica, R. Lefter, I.L. Serban, C. Stefanescu, R. Chirita, The oxidative stress hypothesis in Alzheimer's disease, Free Radic. Biol. Med. 23 (1997) 134–147.

[3] S. Minoshima, Metabolic reduction in the posterior cingulate cortex in very early Alzheimer's disease, Ann. Neurol. 42 (1997) 85–94.

[4] C.R. Jack, M.A. Bernstein, N.C. Fox, P. Thompson, M.W. Weiner, The Alzheimer's Disease neuroimaging initiative (ADNI): MRI methods, J. Magn. Reson. Imag. 27 (2008) 685–691.

[5] R.J. Castellani, M.A. Smith, Compounding artefacts with uncertainty, and an amyloid cascade hypothesis that is 'too big to fail', J. Pathol. 224 (2011) 147–152.

[6] G.M. Shankar, S. Li, T.H. Mehta, A. Garcia-Munoz, D.J. Selkoe, Amyloid β-protein dimers isolated directly from alzheimer brains impair synaptic plasticity and memory, Nat. Med. 14 (2008) 837–842.

[7] E. Karran, M. Mercken, B.D. Strooper, The amyloid cascade hypothesis for Alzheimer's disease: an appraisal for the development of therapeutics, Nat. Rev. Drug Discov. 10 (2011) 698–712.

[8] Anna Tickler, John Wade, Frances Separovic, The role of Aβ peptides in alzheimers disease, Protein Pept. Lett. 12 (2005) 513–519.

[9] D.J. Selkoe, Soluble oligomers of the amyloid beta-protein impair synaptic plasticity and behavior, Behav. Brain Res. 192 (2008) 106–113.

[10] C. Deng, H. Liu, M. Zhang, H. Deng, C. Lei, L. Shen, B. Jiao, Q. Tu, Y. Jin, L. Xiang, A light-up non-thiolated aptasensor for low-mass soluble amyloid-β_{40} oligomers at high salt concentrations, Anal. Chem. 3 (2018) 1433–2402.

[11] Z. Xu, N. Zhang, Y. Zhang, B. Liu, M. Xu, A sensitive gold nanoparticle-based aptasensor for colorimetric detection of $A\beta_{1\text{-}40}$ oligomers, Anal. Methods 10 (2018) 641–645.

[12] S. Judith, F.S. Aileen, T. Charlotte, Methods for the specific detection and quantitation of amyloid-β oligomers in cerebrospinal fluid, J. Alzheimers Dis. Jad 53 (2016) 53–67.

[13] A.D. Keefe, S. Pai, A. Ellington, Aptamers as therapeutics, Nat. Rev. Drug Discov. 9 (2010) 537–550.

[14] Y. Wan, J. Tan, W. Asghar, Y.T. Kim, S.M. Iqbal, Velocity effect on aptamer-based circulating tumor cell isolation in microfluidic devices, J. Phys. Chem. B 115 (2011) 13891–13896.

[15] S. Mackay, D. Wishart, J.Z. Xing, C. Jie, Developing trends in aptamer-based biosensor devices and their applications, IEEE Trans. Biomed. Circuits Syst 8 (2014) 4–14.

[16] T.H. Nguyen, R. Pei, M. Stojanovic, Q. Lin, An aptamer-based microfluidic device for thermally controlled affinity extraction, Microfluid. Nanofluidics 6 (2009) 479–487.

[17] T. Li, R. Fu, H.G. Park, Pyrrolo-dC based fluorescent aptasensors for the molecular recognition of targets, Chem. Commun. 46 (2010) 3271–3273.

[18] X. Li, K. Ma, S. Zhu, S. Yao, Z. Liu, B. Xu, B. Yang, W. Tian, Fluorescent aptasensor based on aggregation-induced emission probe and graphene oxide, Anal. Chem. 86 (2014) 298–303.

[19] N. Duan, S. Wu, X. Ma, Y. Xia, Z. Wang, A universal fluorescent aptasensor based on AccuBlue dye for the detection of pathogenic bacteria, Anal. Biochem. 454 (2014) 1–6.

[20] Y. Zhao, X. Li, Y. Yang, S. Si, C. Deng, H. Wu, A simple aptasensor for $A\beta_{40}$ oligomers based on tunable mismatched base pairs of dsDNA and graphene oxide, Biosens. Bioelectron. 149 (2020) 111840–111846.

[21] Y. Guo, Z. Xiaodong, W. Fu-Gen, A graphene oxide-based switch-on fluorescent probe for glutathione detection and cancer diagnosis, J. Colloid Interface Sci. 530 (2018) 511–520.

[22] W. Hao, W. Yongxiang, J. Jianyu, Y. Ronghua, Gold nanoparticle-based colorimetric and "turn-on" fluorescent probe for mercury(II) ions in aqueous solution, Anal. Chem. 80 (2008) 9021–9028.

[23] M.L.t. Yola, V.K. Gupta, T. Eren, A.E. Åžen, N. Atar, A novel electro analytical nanosensor based on graphene oxide/silver nanoparticles for simultaneous determination of quercetin and morin, Electrochim. Acta 120 (2014) 204–211.

[24] A. Asfaram, M. Ghaedi, S. Agarwal, I. Tyagi, V. Kumar Gupta, Removal of basic dye Auramine-O by ZnS:Cu nanoparticles loaded on activated carbon: optimization of parameters using response surface methodology with central composite design, RSC Adv. 5 (2015) 18438–18450.

[25] R.N. Goyal, V.K. Gupta, S. Chatterjee, A sensitive voltammetric sensor for determination of synthetic corticosteroid triamcinolone, abused for doping, Biosens. Bioelectron. 24 (2009) 3562–3568.

[26] R.S. Swathi, K.L. Sebastian, Resonance energy transfer from a dye molecule to graphene, J. Chem. Phys. 129 (2008) 54700–54703.

[27] N. Duan, S. Wu, X. Ma, X. Chen, Y. Huang, Z. Wang, Gold nanoparticle-based fluorescence resonance energy transfer aptasensor for ochratoxin A detection, Anal. Lett. 45 (2012) 714–723.

[28] H. Karimi-Maleh, F. Tahernejad-Javazmi, N. Atar, M.L.t. Yola, V.K. Gupta, A.A. Ensafi, A novel DNA biosensor based on a pencil graphite electrode modified with polypyrrole/functionalized multiwalled carbon nanotubes for determination of 6-mercaptopurine anticancer drug, Ind. Eng. Chem. Res. 54 (2015) 3634–3639.

[29] Z. Qin, Y. Li, N. Gu, Progress in applications of prussian blue nanoparticles in biomedicine, Adv. Health. Mater 7 (2018) 1800347-180360.

[30] Gautam Milan, Poudel Kishwor, Soon Chul, Jong Yong, Kim Oh, Prussian blue nanoparticles: synthesis, surface modification, and application in cancer treatment, Int. J. Pharm. 549 (2018) 31–49.

[31] H. Chen, M. Yan, X. Wang, Z. Zha, H. Chen, M. Yan, X. Wang, Z. Zha, Multifunctional phase-change hollow mesoporous prussian blue nanoparticles as a NIR light responsive drug Co-delivery system to overcome cancer therapeutic resistance, J. Mater. Chem. B 5 (2017) 7051–7058.

[32] M. Shokouhimehr, E.S. Soehnlen, J. Hao, M. Griswold, C. Flask, X. Fan, J.P. Basilion, S. Basu, S.D. Huang, Dual purpose Prussian blue nanoparticles for cellular imaging and drug delivery: a new generation of T1-weighted MRI contrast and small molecule delivery agents, J. Mater. Chem. 20 (2010) 5251–5259.

[33] F. Yang, S. Hu, Y. Zhang, X. Cai, Y. Huang, F. Wang, S. Wen, G. Teng, N. Gu, A hydrogen peroxide-responsive O_2 nanogenerator for ultrasound and magnetic-resonance dual modality imaging, Adv. Mater. 24 (2012) 5205–5211.

[34] J.F. Keggin, F.D. Miles, Structures and formulæ of the prussian blues and related compounds, Nature 137 (1936) 278–577.

[35] E. Bustos, J. Manríquez, G. Orozco, L.A. Godínez, Preparation, characterization, and electrocatalytic activity of surface anchored, Prussian Blue containing starburst PAMAM dendrimers on gold electrodes, Langmuir 21 (2005) 3013–3021.

[36] K. Sugioka, H. Nakano, M. Nakano, S. Tero-Kubota, Y. Ikegami, Generation of hydroxyl radicals during the enzymatic reductions of the Fe^{3+}-ADP-phosphate-adriamycin and Fe^{3+}-ADP-EDTA systems, Biochim. Biophys. Acta Biomembr. 753 (1983) 411–421.

[37] L. Fan, P. Hao, L. Wang, J. Lu, J. Gao, B. Jiang, X. Zhao, C. Fan, Nanomaterial-based fluorescent DNA analysis: a comparative study of the quenching effects of graphene oxide, carbon nanotubes, and gold nanoparticles, Adv. Funct. Mater. 23 (2013) 4140–4148.

[38] V.K. Gupta, A.K. Singh, L.K. Kumawat, Thiazole Schiff base turn-on fluorescent chemosensor for Al^{3+} ion, Sens. Actuators B 195 (2014) 98–108.

[39] Naveen Mergu, Ashok Singh, Gupta Kumar, Kumar Vinod, Lokesh Kumawat, A reversible fluorescence "off-on-off" sensor for sequential detection of aluminum and acetate/fluoride ions, Talanta 114 (2015) 80–89.

[40] a J. Chen, Q. Wang, L. Huang, H. Zhang, K. Rong, H. Zhang, S. Dong, Prussian blue with intrinsic heme-like structure as peroxidase mimic, Nano Res. 90 (2018) 11446–11452;
b Vázquez-González, Margarita, Torrente-Rodríguez, M. Rebeca, A. Kozell, et al., Mimicking peroxidase activities with prussian blue nanoparticles and their cyanometalate structural analogs, Nano Lett. 17 (2017) 4958–4963.

[41] S.K. Srivastava, V.K. Gupta, S. Jain, Determination of lead using a poly(vinyl chloride)-based crown ether membrane, Analyst 120 (1995) 495.

[42] V.K. Gupta, R. Ludwig, S. Agarwal, Anion recognition through modified calixarenes: a highly selective sensor for monohydrogen phosphate, Anal. Chim. Acta 538 (2005) 213–218.

[43] Deng Chunyan, Zhang Manman, Honghua Liu, Huang Yan, Yang Minghui, Electrostatic force triggering elastic condensation of double-stranded DNA for high-performance one-step immunoassay, Anal. Chem. 90 (2018) 114446-111452.

[44] R. Hurditch, Electrochromism in hydrated tungsten-oxide films, Electron. Lett. 11 (1975) 142–144.

[45] Y. Zhang, W. Yi, L. Yang, L. Di, J. Li, Functionalization of single-walled carbon nanotubes with Prussian blue, Electrochem. Commun. 6 (2004) 1180–1184.

[46] C. Burattini, M. Dell'anna, Monti Campeggi, A FTIR microspectroscopy study of autolysis in cells of the wine yeast Saccharomyces cerevisiae, Vib. Spectrosc. 47 (2008) 139–147.

[47] E.V. Hackl, S.V. Kornilova, L.E. Kapinos, V.V. Andrushchenko, V.L. Galkin, D.N. Grigoriev, Y.P. Blagoi, Study of Ca^{2+}, Mn^{2+} and Cu^{2+} binding to DNA in

solution by means of IR spectroscopy, J. Mol. Struct. 408 (1997) 229–232.
[48] J.M. Domínguez-Vera, C. Enrique, Nanoparticles of Prussian blue ferritin: a new route for obtaining nanomaterials, Inorg. Chem. 42 (2003) 6983–6985.
[49] A.R. Viguera, F.J. Blanco, L. Serrano, The order of secondary structure elements does not determine the structure of a protein but does affect its folding kinetics, J. Mol. Biol. 247 (1995) 670–681.
[50] J. Qin, J.S. Park, D.G. Jo, M. Cho, Y. Lee, Curcumin-based electrochemical sensor of amyloid-β oligomer for the early detection of Alzheimer's disease, Sens. Actuators, B 273 (2018) 1593–1599.
[51] N. Xia, L. Liu, M.G. Harrington, J. Wang, F. Zhou, Regenerable and simultaneous surface plasmon resonance detection of aβ(1-40) and aβ(1-42) peptides in cerebrospinal fluids with signal amplification by streptavidin conjugated to an N-Terminus-Specific antibody, Anal. Chem. 82 (2010) 10151–10157.
[52] W. Xia, T. Yang, G. Shankar, I.M. Smith, D.J. Selkoe, A specific enzyme-linked immunosorbent assay for measuring β-amyloid protein oligomers in human plasma and brain tissue of patients with alzheimer disease, Arch. Neurol. 66 (2009) 190–199.